Steric and electronic influence of Re(I) tricarbonyl complexes with various coordinated β-diketones

Amanda-Lee Ezra Manicum[a], Marietjie Schutte-Smith[b*], Frikkie Malan[c] and Hendrik Gideon Visser[b]

[a] Department of Chemistry, Tshwane University of Technology, PO Box X680, Pretoria, 0001, South Africa
[b] Department of Chemistry, University of the Free State, PO Box X339, Bloemfontein, 9300, South Africa
[c] Department of Chemistry, University of Pretoria, 02 Lynnwood Road, Hatfield, Pretoria 0001, South Africa

* schuttem@ufs.ac.za, +27 51 401 9896

Highlights

- DFT computational study on β-diketone rhenium(I)-tricarbonyl complexes.
- •'2+1' mixed ligand reactions of *fac*-[$Re(CO)_3(OO')(PCy_3)$] (OO' = acetylacetone derivatives).
- Solid state structures and evaluation of intra- and intermolecular interactions.
- A systematic trend is observed in the experimental and computational study.

Abstract

Re(I) tricarbonyl complexes, with coordinated β-diketones, are the center of attention as they form part of a library of promising cancer therapeutic and diagnostic agents. In this study, we present three new Re(I) crystal structures. {*fac*-[$Re(Benzac)(CO)_3(PCy_3)$] (**4**), *fac*-[$Re(Tfaa)(CO)_3(PCy_3)$] (**5**), and *fac*-[$Re(Hfaa)(CO)_3(PCy_3)$] (**6**); benzoylacetone = Benzac; trifluoroacetylacetone = Tfaa and hexafluoroacetylacetone = Hfaa; PCy_3 = tricyclohexylphosphine}. The three reported complexes were synthesized with ease and good yield, involving the "2 + 1" mixed ligand approach. The complexes were characterized using analytical tools: IR, NMR, UV/Vis, single-crystal X-ray diffraction. The Tolman cone angles (θ) were calculated as 141.93°, 148.77°, and 149°; and compared to the Equivalent cone angles obtained from DFT calculations. These were 131.25°, 134.34°, and 134.28° for (**4**), (**5**), and (**6**), respectively. The DFT analysis observed that the Re-P bond distances decrease as the number of electron-withdrawing groups (CF_3) on the β-diketonato ligands increase. In general, the theoretical and experimental Re-P and Re-O_{OO} bond distances compared well among the complexes**,** with the most

significant deviation occurring for **4** (relative differences of 0.055 Å (Re-P) and 0.015 Å (average Re-O)). Hirshfeld surface analysis was used to obtain the fingerprint plots, and the Hirshfeld surfaces were mapped with d_{norm} for **4**, **5**, and **6**.

Graphical abstract

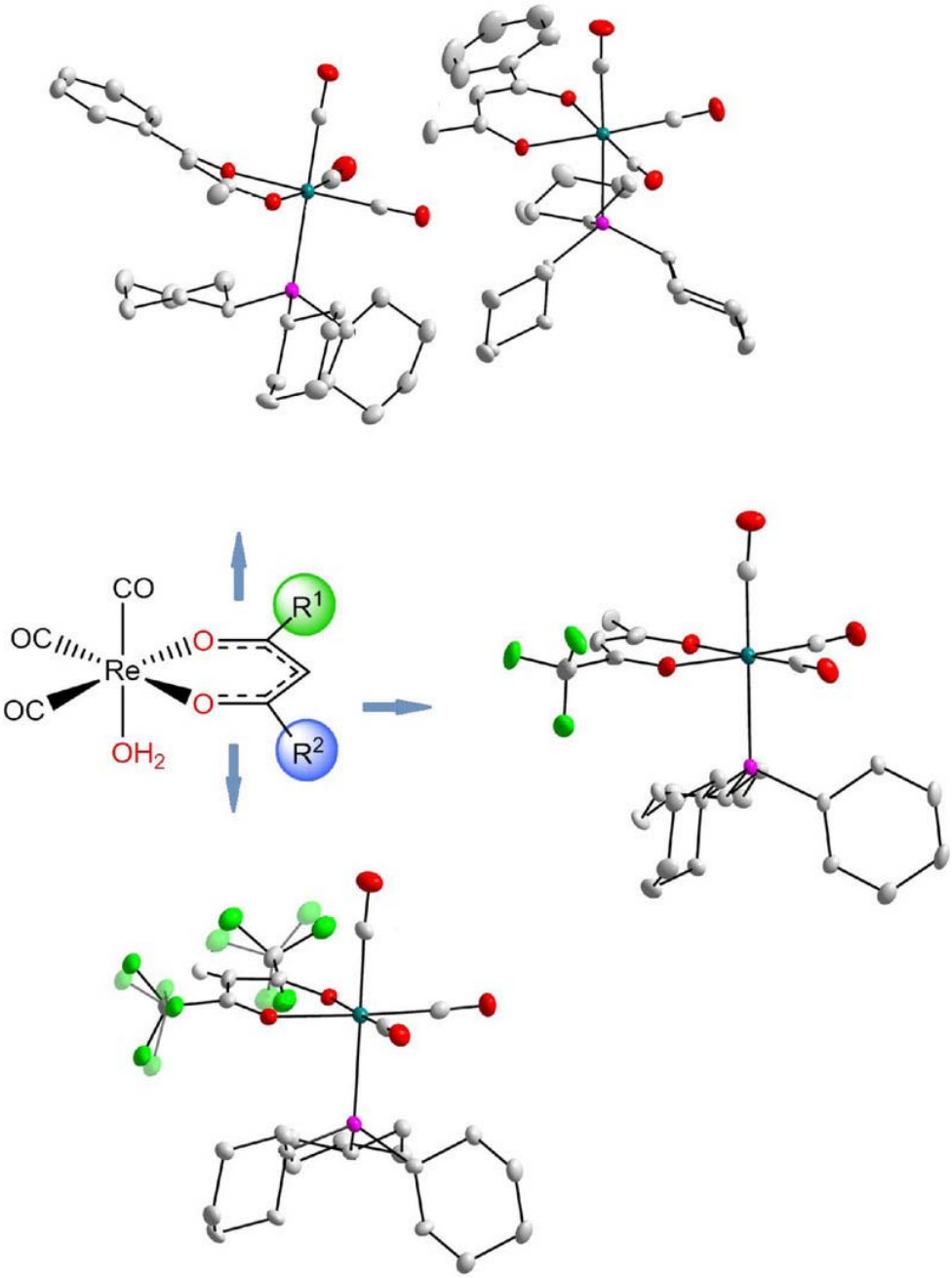

Key words: Re(I) tricarbonyl, β-diketones, tricyclohexylphosphine, Tolman cone angle, DFT calculations

1. Introduction

For several reasons, interest in rhenium(I) complexes has increased over the last years. In medical applications, rhenium(I) complexes are investigated for uses ranging from the photocatalytic release of CO (photoCORMS) to radiopharmaceutical diagnostics and treatment of cancer, chemotherapy, anti-microbial properties, and photodynamic therapy (PDT).[1,2,3,4,5,6,7,8,9,10,11,12,38]

The *fac*-$[Re(OH_2)_3(CO)_3]^+$ precursor is very flexible for designing molecules with various properties and employing different coordination models like the '2 + 1' and the more recently introduced '2 + 1 + 1' mixed ligand approach.[7,13,14,15,16,17,18] On the other hand,β-diketones are popular among researchers interested in radiopharmaceutical or chemotherapeutic applications *fac*-$Re(CO)_3^+$ synthon, because it can easily be modified to attach target biomolecules on its backbone. [2,19,40]

Our laboratory has mainly focused on understanding the intimate mechanism of substitution reactions, using various combinations of ligands, to better understand the behaviour of these complexes in biological systems and to evaluate various structure-property relationships. [20,41,42,46,47]

This paper presents the synthesis of Re(I) tricarbonyl complexes with altered β-diketone ligands with tricyclohexylphosphine completing the octahedral environments. The synthesis, characterization, single-crystal X-ray diffraction solid-state structures, Tolman cone angle, and density functional calculations (DFT) of the corresponding Re(I) complexes which are of the form *fac*-[Re(*O,O'*-bid)$(CO)_3(PCy_3)$] is reported (*O,O'*-bid = BenzacH = benzylacetylacetone, TfaaH = trifluoroacetylacetone, HfaaH = hexafluoroacetylacetone)

2. Materials and methods

2.1. Experimental

Analytical grade reagents and solvents were used for this investigation, procured from Sigma-Aldrich, and used without additional purification. The rhenium pentacarbonyl bromide used to prepare the precursor, *fac*-$[NEt_4]_2[ReBr_3(CO)_3]$, was purchased from Strem Chemicals, Newburyport, Massachusetts, United States of America.

fac-$[NEt_4]_2[ReBr_3(CO)_3]$ was synthesized according to a published procedure.[21] The

NMR data were obtained from a Bruker AXS 600 MHz (operating at 600.28 and 150.96 MHz for ^{1}H and ^{13}C, respectively) or Bruker AXS 300 MHz (operating at 121.49 MHz for ^{31}P) nuclear magnetic resonance spectrometer at room temperature, using the stated deuterated solvents. The chemical shifts, δ, are reported in ppm with ^{1}H and ^{13}C spectra primarily calibrated relative to the residual CD_2Cl_2 (5.32; 53.5 ppm) peaks. The ^{31}P NMR spectra were calibrated relative to 85% H_3PO_4 as external standard in a capillary (0 ppm). All coupling constants, *J*, are reported in Hertz (Hz). The infrared spectra were recorded at room temperature on a Bruker Tensor 27 Standard System spectrophotometer (4000–370 cm^{-1} region) utilizing a He-Ne laser at 632.6 nm (3000–600 cm^{-1} region). Solid-state samples were analyzed as KBr pellets with ν_{CO} = stretching frequency of the carbonyl ligands coordinated to the metal center. A Varian Cary 50 Conc. UV-Visible Spectrophotometer was used for UV-Vis spectra data collections conducted in a 1.000 ± 0.001 cm quartz cuvette cell. The UV-Vis spectrophotometer was equipped with a Julabo F12-mV temperature cell regulator, accurate to 0.1 °C. The program used for the computational calculation of the Equivalent cone angle is Solid-G. Version 0.25 2006. Complexes *fac*-[Re(Benzac)$(CO)_3(H_2O)$] (**1**), *fac*-[Re(Tfaa)$(CO)_3(H_2O)$] (**2**) and *fac*-[Re(Hfaa)$(CO)_3(H_2O)$] (**3**) were prepared according to the procedure found in the literature.[39,40] Additionally, the synthesis of *fac*-[Re(Benzac)$(CO)_3(PCy_3)$] (**4**), *fac*-[Re(Tfaa)$(CO)_3(PCy_3)$] (**5**) and *fac*-[Re(Hfaa)$(CO)_3(PCy_3)$] (**6**) is illustrated in Figure 9.

2.1.1. Synthesis and characterization of Re(I) complexes

fac-[Re(Benzac)$(CO)_3(PCy_3)$] (**4**)

1 (45 mg; 0.1 mmol) was dissolved in methanol (3 ml), and PCy_3 (27 mg; 0.1 mmol) dissolved in methanol (2 ml) was added. The solution was then stirred for 7 hours at room temperature, and the bright yellow solution was left to crystallize.

Yield = 60 mg, 84%

IR (KBr, cm^{-1}): ν_{CO} = 2021, 1927, 1909

^{1}H NMR (600 MHz, dichloromethane-*d*2): δ 7.85 (d, *J* = 7.8 Hz, 2H), 7.61 (d, *J* = 7.9 Hz, 1H), 7.34 (q, *J* = 7.8 Hz, 2H), 6.17 (s, 1H), 2.12 (s, 3H), 2.10 – 2.00 (m, 6H), 1.97 (d, *J* = 11.1 Hz, 6H), 1.78 (dd, *J* = 20.9, 9.6 Hz, 8H), 1.64 (d, *J* = 7.6 Hz, 3H), 1.59 – 1.45 (m, 9H), 1.34 (t, *J* = 7.1 Hz, 1H)

^{13}C NMR (150.96 MHz, dichloromethane-*d*2): δ 191.39, 181.65, 138.12, 134.14, 131.22, 130.44, 128.50, 128.30, 128.06, 127.10, 99.03, 34.28, 29.22, 28.06, 27.84, 26.31

^{31}P NMR (121.49 MHz, dichloromethane-*d*2): δ 21.47

UV/Vis: ε(λmax = 375 nm) = 1 964 M^{-1} cm^{-1}

Tolman cone angle (θ): 141.93°

Equivalent cone angle (θ°): 131.25°

fac-[Re(Tfaa)$(CO)_3$(PCy_3)] (**5**)

2 (22 mg; 0.05 mmol) was dissolved in methanol (3 ml) and PCy_3 (14 mg; 0.05 mmol) dissolved in 2 ml methanol was added. The reaction mixture was stirred for 8 hours at room temperature, and a yellow precipitate formed that was filtered off and dried. The yellow filtrate was left to crystallize, and crystals for the collection with X-ray diffraction formed.

Yield = 20 mg, 57%

IR (KBr, cm^{-1}): ν_{CO} = 2016, 1930, 1892

^{1}H NMR (600 MHz, dichloromethane-*d2*): δ 5.86 (s, 1H), 2.13 (d, *J* = 10.3 Hz, 3H), 2.11 – 2.00 (m, 4H), 1.91 (d, *J* = 30.9 Hz, 8H), 1.88 – 1.77 (m, 8H), 1.72 (d, *J* = 20.5 Hz, 4H), 1.56 (s, 1H), 1.52 – 1.31 (m, 8H)

^{13}C NMR (150.96 MHz, dichloromethane-*d2*): δ 206.51, 197.01, 191.86, 169.33, 119.01, 117.13, 98.46, 34.35, 30.67, 29.29, 28.77, 27.90, 27.59, 26.94, 26.69, 26.61, 26.30, 26.19, 26.09, 25.82

^{31}P NMR (121.49 MHz, dichloromethane-*d2*): δ 22.73

UV/Vis: ε(λ_{max} = 325 nm) = 2 937 M^{-1} cm^{-1}

Tolman cone angle (θ): 148.77°

Equivalent cone angle (θ°): 134.34°

fac-[Re(Hfaa)$(CO)_3$(PCy_3)] (**6**)

3 was dissolved in methanol (3 ml), and PCy_3 (28 mg; 0.1 mmol) dissolved in 2 ml methanol was added. The solution was stirred for 6 hours at room temperature, and the orange solution was left to crystallize.

Yield = 48 mg, 63%

IR (KBr, cm^{-1}): ν_{CO} = 2027, 1936, 1904

^{1}H NMR (600 MHz, dichloromethane-*d2*): δ 6.25 (s, 1H), 2.11 (s, 1H), 2.00 – 1.76 (m, 15H), 1.76 – 1.56 (m, 4H), 1.47 – 1.35 (m, 4H), 1.25 (t, *J* = 7.5 Hz, 9H)

^{13}C NMR (150.96 MHz, dichloromethane-*d2*): δ 174.14, 117.68, 92.14, 34.91, 29.29, 27.58, 26.92, 26.54, 26.30, 26.21, 25.78, 25.66, 25.38

^{31}P NMR (121.49 MHz, dichloromethane-*d2*): δ 23.68

UV/Vis: $\varepsilon(\lambda_{max} = 365\ nm) = 1\ 898\ M^{-1}\ cm^{-1}$

Tolman cone angle (θ): 149.00°

Equivalent cone angle (θ°): 134.28°

2.2.Crystallography

The crystal structure of **5** was collected on a Bruker D8 Quest Eco Chi Photon II CPAD diffractometer, **4** and **6** were collected on a Bruker D8 Venture 4K Kappa Photon III C28 diffractometer. Crystal Explorer 2.1 was used to perform the Hirshfeld surface analysis; the Hirshfeld surfaces mapped with d_{norm} and the colored 2D fingerprint plots of **4**, **5**, and **6** were obtained.[48] All the cell refinements and data reduction were completed using SAINT-Plus and XPREP.[22] To correct the absorption effects, the multi-scan technique and software package SADABS were used.[22] All the crystal structures were solved using the direct method package SIR-97[23] and refined by using WinGX[24] and SHELXL-97.[25] The crystal structures' graphical representation was obtained with the program DIAMOND.[26] The structures are shown with thermal ellipsoids drawn at a 50% probability level unless otherwise stated. A summary of the general crystal data and refinement parameters for complexes **4**, **5** and **6** are given in Table 2.

2.3. Computational chemistry

All calculations were carried out using Density Functional Theory (DFT) using the B3LYP-D3 (B3LYP with the Grimme empirical dispersion correction D3) hybrid functional,[27,28] as implemented in the Orca package 4.2.0.[29] The triple-ζ basis set def2-TZVPP was used for all atoms.[30] The ORCA calculations were accelerated using the RI approximation for the Coulomb integrals (RI-J),[31] while the exchange terms were computed using the "chain-of-spheres" (COSX) approximation.[32] The geometries of all compounds were fully optimised without any symmetry restrictions, ensuring that the local minima had zero imaginary vibrational frequencies and

providing the thermal correction to free energies at 298.15 K and 1 atm. All calculations were performed in dichloromethane (ε = 8.93) as the solvent and corresponded to the solvent in which a specific compound was dissolved as part of the NMR studies. Simulated NMR spectra were calculated using the same level of theory and respective implicit solvent model in the standard Orca framework applying the gauge-including atomic orbital (GIAO) method.[33] The relative ^{1}H, ^{13}C, and ^{31}P chemical shifts (δ_H, δ_C, δ_P) were estimated using the corresponding internal standard (TMS for ^{1}H and ^{13}C, H_3PO_4 for ^{31}P) shielding calculated at the same level of theory and again using the same implicit solvent model. Scaling of the data was done in accordance with Zhang *et al.*, Benassi, and Lodewyk *et al.*[34,35,36] All energies used and reported in this work are zero-point vibrational-corrected. Visualization was done using Chemcraft software.[37]

3. Results and Discussion

3.1. Synthesis

The synthesis of three Re(I) tricarbonyl complexes is reported (**4**, **5,** and **6**), and the three precursor complexes (**1**, **2,** and **3**) were synthesized as reported in the literature.[38,39,40] The complexes were obtained in good yield (84%, 57%, and 63% for **4**, **5,** and **6,** respectively), and the synthetic method utilized is relatively straightforward. The IR spectra of the synthesized Re(I) tricarbonyl complexes display the characteristic carbonyl stretching frequencies in the range 2027-1892 cm^{-1} as summarised in Table 1.[41] The carbonyl stretching frequency of the Hfaa complex is the most prominent, signifying the effect of the fluoro atoms on the ligand backbone, possibly because the higher electron-withdrawing ability of Hfaa decreases the electron density on the metal and results in strengthening of the C≡O bond. The NMR spectra were obtained from deuterated dichloromethane. The ^{1}H and ^{13}C NMR data obtained are consistent with some complexes' proposed structures and existing literature data.[42] Upon coordination of the Benzac, Tfaa, and Hfaa, the characteristic shifts are noticeable, compared to their non-coordinated states. The ^{31}P NMR data displayed systematic downfield single peaks (at 21.47, 22.73, and 23.68 for **4**, **5,** and **6,** respectively), proving the absence of isomers. Additionally, the ^{31}P NMR data again shows the electron-withdrawing effects of the fluoro atoms on the backbones of **5** and **6**, resulting in a downfield ^{31}P-shift.

The Tolman cone angles (θ) of the coordinated PCy_3 ligands were calculated according to the literature, as illustrated in Figure 1a.[43] The θ of **4**, **5,** and **6** were calculated as 141.93°, 148.77°, and 149.00°, respectively, which correlates well with data reported in the literature.[39] Furthermore, the θ of **5** and **6** is approximately 149° which displays the sizeable steric bulk of PCy_3. **4** has the smallest θ of 141.93°, which is possibly due to the steric effect from the phenyl ring on the Benzac ligand backbone, narrowing the cavity for the phosphine to coordinate. Moreover, the same trend is seen in the computational calculation of the Equivalent cone angle (θ°).[44] The Equivalent cone angle (θ°) is the percentage of the metal coordination sphere occupied by a given ligand in an organometallic or coordination complex, and Figure 1b is an illustration of graphics obtained from doing Solid-G calculations. θ° is smaller than θ because the program does not assume free rotation about the M-L axis. The angles of **4**, **5,** and **6** were calculated to be 131.25°, 134.34°, and 134.28°. Again, **4** has the smallest θ° of 131.25°, proving that the phenyl entity on Benzac could cause the barrier and steric interference for coordination.

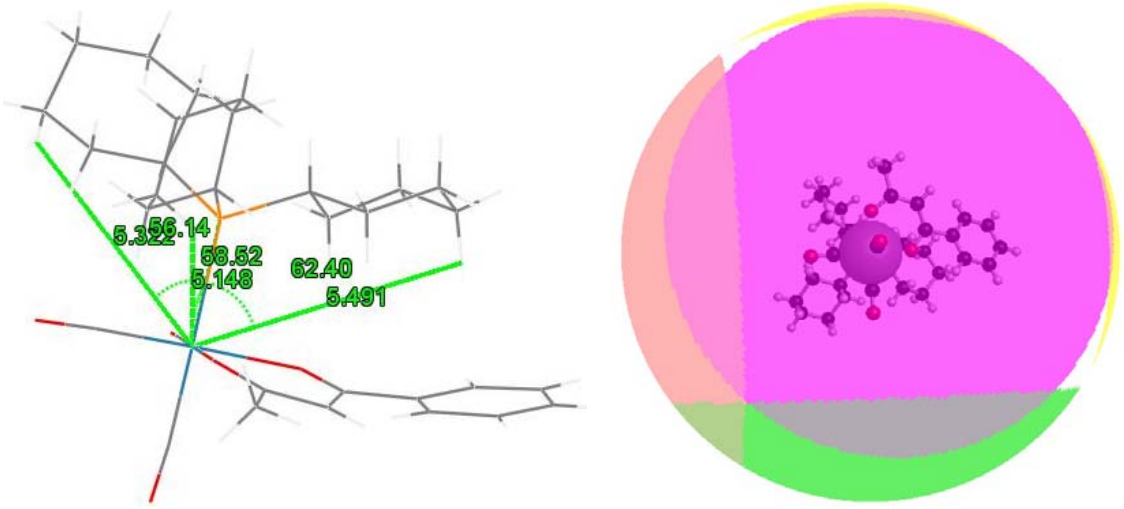

(a) **(b)**

Figure 1: (a) Illustration of the Tolman cone angle calculation (θ) and (b) the Equivalent cone angle (θ°) bulk image of **4**.

Table 1: Spectroscopic and steric data for complexes **4** - **6**.

Complexes	ν_{CO} (cm^{-1})	^{31}P δ (ppm)	λ_{max} (nm)	ε (M^{-1} cm^{-1})	Tolman Cone Angle (θ)	Equivalent Cone Angle (θ°)
4	2021, 1927, 1909	21.47	375	1 964	141.93	131.25
5	2016, 1930, 1892	22.73	325	2 937	148.77	134.34
6	2027, 1936, 1904	23.68	365	1 898	149.00	134.28

3.2. Crystallography

The crystal structures of *fac*-[Re(Benzac)$(CO)_3(PCy_3)$] (**4**), *fac*-[Re(Tfaa)$(CO)_3(PCy_3)$] (**5**), and *fac*-[Re(Hfaa)$(CO)_3(PCy_3)$] (**6**) were obtained from the slow evaporation of acetone solutions. The crystal data of **4**, **5**, and **6** are presented in Table 2, and the molecular diagrams illustrating the numbering scheme are given in Figure 2.

fac-[Re(Benzac)$(CO)_3(PCy_3)$] (**4**) crystallised in the triclinic $P\bar{1}$ space group with two molecules in the asymmetric unit. All the bond distances and angles are within the normal range, with selected bond distances for (**4**), (**5**) and (**6**) summarised in Table 3.[38,39,40,41,42,45,46,47] The octahedral geometry is slightly distorted and is confirmed by the following most prominent outliers: C3A-Re1A-C1A and O4A-Re1A-O5A with angles of 87.47(13) ° and 84.12(8) ° and P1B-Re1B-C2B and O4B-Re1B-O5B with angles of 96.22(11) ° and 83.72(8) ° respectively.

Table 2: Summary of crystal data of *fac*-[Re(Benzac)$(CO)_3(PCy_3)$] (**4**), *fac*-[Re(Tfaa)$(CO)_3(PCy_3)$] (**5**), and *fac*-[Re(Hfaa)$(CO)_3(PCy_3)$] (**6**).

	4	**5**	**6**
Empirical formula	$C_{31}H_{42}O_5PRe$	$C_{26}H_{37}F_3O_5PRe$	$C_{26}H_{34}F_6O_5PRe$
Formula weight (g mol^{-1})	711.83	703.72	757.7
Crystal system	Triclinic	Monoclinic	Monoclinic
Space group	$P\bar{1}$	$P2_1/c$	$P2_1/c$
a (Å)	9.922(2)	9.1356(11)	9.2609(7)
b (Å)	18.055(4)	33.762(4)	33.608(2)
c (Å)	19.009(5)	9.2315(12)	9.3712(7)
α (°)	62.485(8)	90	90
β (°)	87.039(9)	106.007(4)	106.717(2)
γ (°)	84.961(9)	90	90
Volume (A^3)	3008.3(13)	2737.0(6)	2793.4(4)
Z	4	4	4
ρ_{calc} (g cm^{-3})	1.574	1.708	1.802
Crystal colour	Yellow	Yellow	Orange
Crystal morphology	Plate	Cuboid	Plate
Crystal size (mm)	0.067 x 0.095 x 0.189	0.120 x 0.270 x 0.430	0.029 x 0.089 x 0.223
μ (mm^{-1})	4.129	4.552	4.482
F (000)	1432	1400	1496
θ range (°)	2.27 - 28.36	2.84 - 28.31	2.42 - 28.29
Index ranges	-13 ≤ h ≤ 13	-12 ≤ h ≤ 12	-12 ≤ h ≤ 10
	-23 ≤ k ≤ 23	-44 ≤ k ≤ 44	-44 ≤ k ≤ 44
	-25 ≤ l ≤ 25	-12 ≤ l ≤ 12	-12 ≤ l ≤ 12
Reflections collected	122487	73558	63361
Unique reflections	14506	6605	6747
Reflections with I > 2σ(I)	12261	6549	6293
R_{int}	0.0772	0.0433	0.0561
Completeness to 2 theta (°, %)	27.999, 100	27.999, 99.5	27.999, 99.9
Data/restraints/parameters	14506/0/695	6605/0/331	6747/0/346
GooF	1.06	1.246	1.352
R [I > 2σ(I)]	*R*1 = 0.0248	*R*1 = 0.0388	*R*1 = 0.0453
	w*R*2 = 0.0544	w*R*2 = 0.0834	w*R*2 = 0.0910
R (all data)	*R*1 = 0.0352	*R*1 = 0.0389	*R*1 = 0.0492
	w*R*2 = 0.0612	w*R*2 = 0.0835	w*R*2 = 0.0925
ρ_{max}, ρ_{min} (e A^{-3})	1.678, -0.995	5.108, -2.242	2.09, -3.506

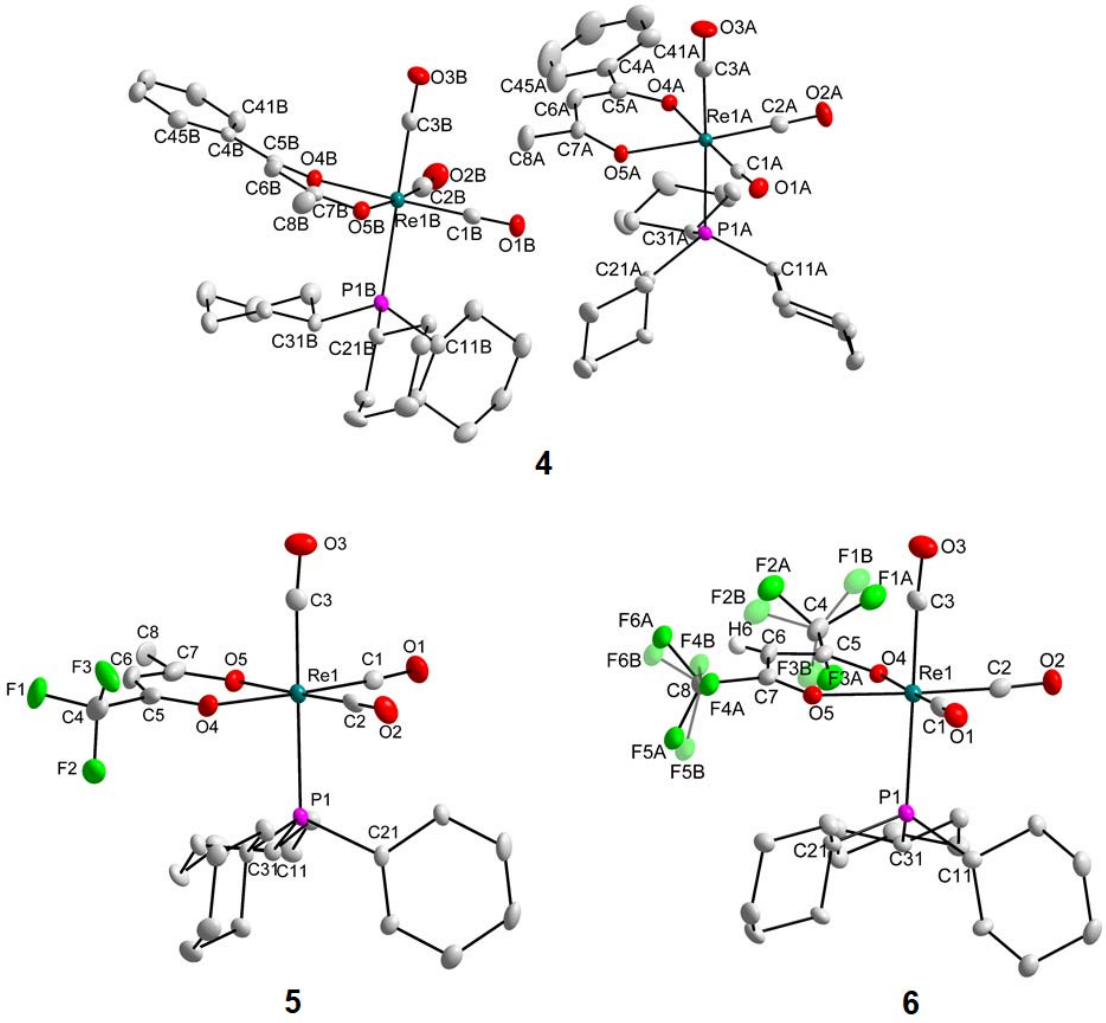

Figure 2: Molecular diagrams of **4**, **5**, and **6** illustrating the numbering scheme used. Hydrogen atoms and the numbering of some of the carbon atoms in the tricyclohexyl rings are omitted for clarity. Ellipsoids are drawn at a 50% probability level.

The acetylacetonato backbone in both molecules tend to bend away from the PCy_3 ligand, towards the axial carbonyl ligand (C3), and dihedral angles of 13.9(1) ° and 16.8(1) ° are calculated between the planes through Re1,C1,O1,C2,O2,O4,O5 (rms 0.0199 for A and 0.0194 for B) and O4,O5,C5,C6,C7 (rms 0.0368 for A and 0.0259 for B) for molecule A and B respectively. Eleven C-H…O hydrogen bonding interactions (eight intramolecular and three intermolecular) and one intramolecular π-interaction are observed in the structure of **4**. They are summarized and illustrated in Table 4 and Figure 3, respectively. In addition, bifurcation occurs in molecule B, where O4B is the acceptor atom in three intramolecular hydrogen bonding interactions (C32B-H32D…O4B, C36B-H36D…O4B, C41B-H41B…O4B).

Table 3: Summary of selected bond distances (Å) for *fac*-[Re(Benzac)$(CO)_3(PCy_3)$] (**4**), *fac*-[Re(Tfaa)$(CO)_3(PCy_3)$] (**5**), and *fac*-[Re(Hfaa)$(CO)_3(PCy_3)$] (**6**).

Description		Complex			
		4			
		(Molecule A)	**(Molecule B)**	**5**	**6**
Bond distances (Å)	Re1-C1	1.898(3)	1.899(3)	1.912(5)	1.897(6)
	Re1-C2	1.904(3)	1.903(3)	1.905(5)	1.906(6)
	Re1-C3	1.955(3)	1.944(3)	1.948(5)	1.956(6)
	Re1-O4	2.132(2)	2.128(2)	2.147(3)	2.164(4)
	Re1-O5	2.137(2)	2.130(2)	2.156(3)	2.153(4)
	Re1-P1	2.5151(9)	2.5285(9)	2.5319(12)	2.5172(14)

fac-[Re(Tfaa)$(CO)_3(PCy_3)$] (**5**) crystallised in the monoclinic $P2_1/c$ space group with one molecule in the asymmetric unit. The bond distances and angles compare well to the structure of **4** and similar structures in literature.[38,39,40,41,42,45,46,47]

The octahedron is also slightly distorted with the bite angle (O4-Re1-O5) reported as 83.85(15) ° and C1-Re1-O4 reported as 174.85(17) °; these angles deviate the most from the ideal 90 ° and 180 ° respectively. Once again, the acetylacetonato ligand bend away from the PCy_3 ligand with a dihedral angle of 10.3(2) ° reported between the plane through Re1,C1,O1,C2,O2,O4,O5 (rms 0.0168) and the plane through O4,O5,C5,C6,C7 (rms 0.0203). Three hydrogen bonding interactions (two intra- and one intermolecular) and one intramolecular π-interaction is observed in the structure of **5** and are illustrated and summarised in Figure 3 and Table 4, respectively.

Table 4: Summary of interactions observed in the structures of **4**, **5** and **6**.

D–H…A	d (D–H) (Å)	d (H…A) (Å)	d (D…A) (Å)	D–H…A angle (°)
		4		
C12-H12B…O2A[a]	0.99	2.58	3.382(4)	138
C15A-H15B…O3A[b]	0.99	2.57	3.290(4)	130
C16A-H16A…O1A	0.99	2.51	3.481(4)	166
C21A-H21A…O1B	1.00	2.55	3.543(5)	171
C22A-H22B…O5A	0.99	2.47	3.215(4)	132
C22B-H22D…O5B	0.99	2.51	3.178(4)	124
C32A-H32A…O4A	0.99	2.43	3.257(4)	141
C32B-H32D…O4B	0.99	2.56	3.378(4)	140
C36B-H36D…O4B	0.99	2.50	3.338(5)	142
C41B-H41B…O4B	0.95	2.35	2.678(5)	100
C43B-H43B…O1A[c]	0.95	2.59	3.496(5)	158
C34A-H34B…Cg2		2.80[e]	3.754(4)[f]	163[g]
		5		
C6-H6…F1	0.98(7)	2.29(7)	2.678(8)	103(4)
C23-H23A…O2[d]	0.99	2.59	3.484(6)	150
C36-H36B…O4	0.99	2.45	3.158(6)	128
C12-H12A…Cg1		2.79[e]	3.607(5)[f]	140[g]
		6		
C6-H6…F2A	0.76(8)	2.47(7)	2.770(10)	105(7)
C6-H6…F2B	0.76(8)	2.27(7)	2.640(12)	111(7)
C6-H6…F6B	0.76(8)	2.36(8)	2.692(13)	108(6)
C22-H22B…O5	0.99	2.46	3.150(7)	127
C32-H32B…O4	0.99	2.57	3.417(7)	144

[a] 1-x,-y,2-z; [b] 1+x,y,z; [c] -1+x,1+y,z; [d] –x,-y,-z; [e] d(H…Cg); [f] d(D…Cg); [g] D-H…Cg angle;Cg1 = centroid of Re1,O4,O5,C5,C6,C7; Cg2 = centroid of C4A,C41A,C42A,C43A,C44A,C45A.

fac-[Re(Hfaa)$(CO)_3(PCy_3)$] (**6**) crystallised in the $P2_1/c$ monoclinic space group with one molecule in the asymmetric unit, with all the bond distances and angles within the normal range.[38,39,40,41,42,45,46,47] The octahedral geometry around the rhenium centre is again slightly distorted, with the most considerable deviations from the ideal 90 ° being the bite angle O4-Re1-O5 (83.89(15)) ° and O4-Re1-P1 (94.67(11)) °. Both trifluoro groups are positionally disordered in a 44.10:55.90 (F1, F2, and F3) and 41.85:58.15 (F4, F5, and F6) ratio. In **6**, the acetylacetonato backbone also 'bends' slightly away from the PCy_3 ligand with a dihedral angle of 15.0(2) ° between the plane through Re1,C1,O1,C2,O2,O4,O5 (rms 0.0227) and the plane through O4,O5,C5,C6,C7 (rms 0.0275). Five intramolecular hydrogen bonding interactions are observed in the structure of **6** and are illustrated in Figure 3 and summarised in Table 4. Bifurcation occurs at the donor atom H6, taking part in three intramolecular interactions to F2A, F2B, and F6B. Four F…O short contacts is also observed in **6** with

distances varying between 2.826(11) Å and 2.989(11) Å; F6A and F6B to O2 (1+x,y,1+z) and F2A and F2B to O3 (x,3/2-y,1/2+x) and is illustrated in Figure S1 in the supplementary file.

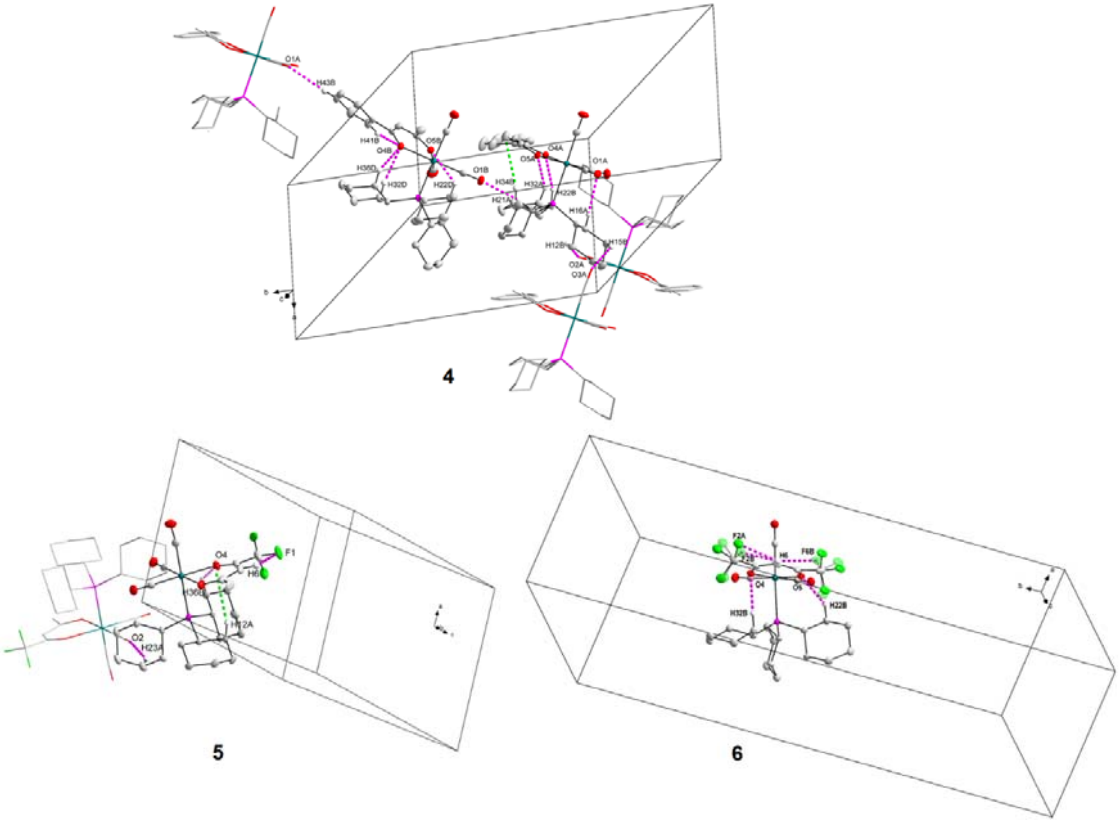

Figure 3: Illustration of the intermolecular interactions observed in structures **4**, **5**, and **6**. Hydrogen atoms and some atom labels are omitted for clarity.

All of the donor atoms in the hydrogen bonding interactions in **4**, **5**, and **6** are carbon atoms in the cyclohexyl and benzyl ring systems, except for C6 in **5** and **6** that forms interactions with the fluoro atoms. In **4**, where there are no fluoro atoms, C6 is not involved in any interactions. The trend in the dihedral angle between the plane through Re1,C1,O1,C2,O2,O4,O5 and the plane through O4,O5,C5,C6,C7 is as follows: **5** (10.3(2) °) < **6** (15.0(2) °) ≤ **4** (13.9(1) ° and 16.8(1) °).

All the Re-O bond distances are within the same range, varying between 2.128(2) Å (shortest observed in **4**) and 2.164(4) Å (longest observed in **6**), displaying somewhat of an electronwithdrawing effect of the fluoro atoms on the bond distances in the solid state structures. Bond distances of Re1-P1 range from 2.5151(9) Å (shortest noted in **4**) to 2.5319(12) Å (longest noted in **6**), which is considered normal. The systematic

increasing trend in the Re1-C3 bond distances are as follows: (**4**) Molecule B < (**5**) < (**4**) Molecule A < (**6**) as the fluoro atoms increase on the diketone ligand backbone.

3.3. Hirshfeld surface analysis

Fingerprint plots of the crystal structures of **4**, **5**, and **6** were obtained and are illustrated in Figure 4. Fingerprint plots can be decomposed to highlight particular atom pair close contacts and enable the separation of contributions from the different interaction types, which otherwise overlap in the full fingerprint plot. Complementary regions are visible in each plot where one molecule act as the donor ($d_e > d_i$) and the other molecule act as the acceptor ($d_e < d_i$) (with d_e and d_i the distance from a certain point on the surface to the nearest nucleus outside and inside the surface respectively).[48,49]

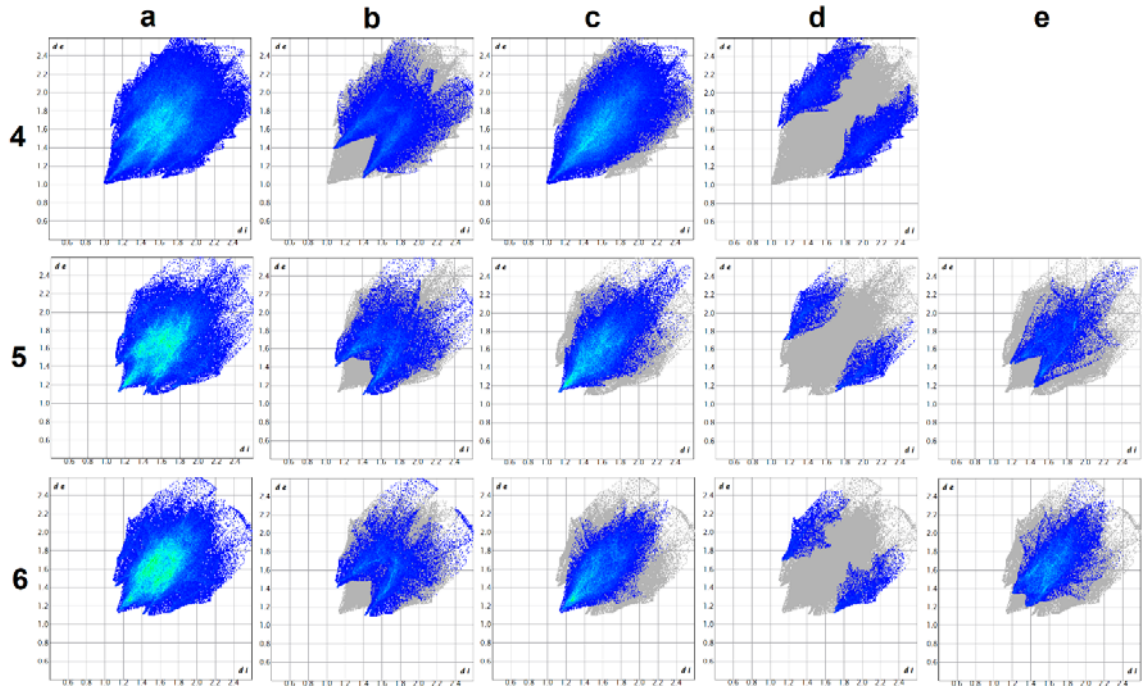

Figure 4: Fingerprint plots of 4, 5, and 6 with (a) illustrating the full fingerprint, (b) the fingerprint plots resolved into H…O/O…H contacts, (c) the fingerprint plots resolved into H…H contacts, (d) the fingerprint plots resolved into H…C/C…H contacts, and (e) the fingerprint plots resolved into H…F/F…H contacts.

The fingerprint plots for each type of interaction have the same pattern for **4**, **5**, and **6,** as illustrated in Figure 4. In the structure of **4**, the H…O/O…H interactions comprise 23.6%, the H…H interactions comprise 63.5%, and the H…C/C…H interactions

comprise 12.8% of the total Hirshfeld surface area. In **5**, the H…O/O…H interactions comprise 25.3%, the H…H interactions comprise 47.6%, the H…C/C…H interactions comprise 7.6%. The H…F/F…H interactions comprise 15.8% while in **6**, the H…O/O…H interactions comprise 20.3%, the H…H interactions comprise 34.4%, the H…C/C…H interactions comprise 5.9%. The H…F/F…H comprises 26.8% of the total Hirshfeld surface area. The overall contribution of the H…H contacts varies the most, from 63.5% to 34.4%, but it contributes the most to the crystal packing in **4**, **5**, and **6**. Another substantial amount of stabilization in **4**, **5**, and **6** comes from the H…O/O…H interactions, while the H…F/F…H contacts significantly stabilize **6** (26.8%) and to some degree in **5** (15.8%).

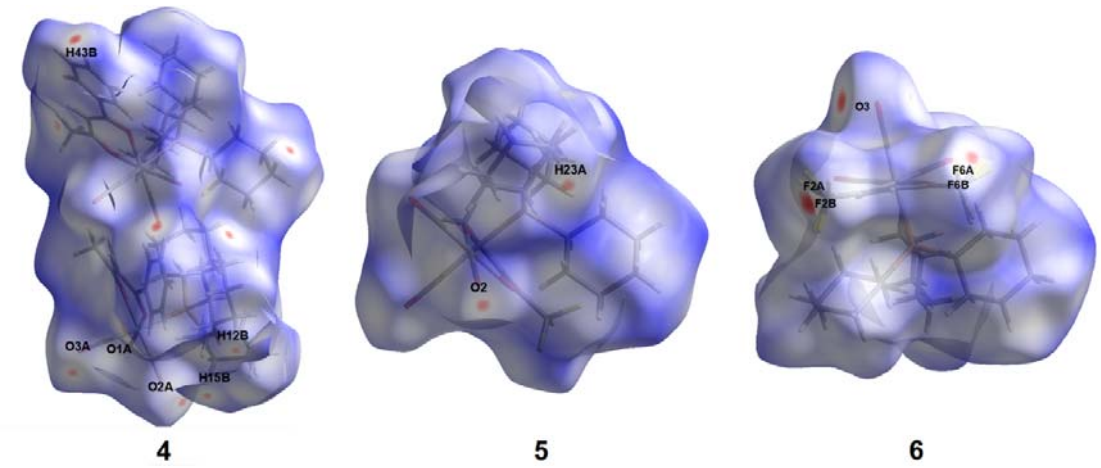

Figure 5: Hirshfeld surfaces for **4**, **5**, and **6** mapped with d_{norm} over the range -0.15 to 1.8.

When d_{norm} (as defined and discussed by Spackman & Jayatilaka) is mapped on a Hirshfeld surface, intermolecular contacts, defined as contacts shorter than the sum of the van der Waals radii, appear as red spots on a predominantly blue surface; this is a valuable and unbiased method to identify close intermolecular contacts, even in complex crystal structures.[49]

A d_{norm} Hirshfeld plot of **4**, **5**, and **6** are presented in Figure 5, indicating the red spots associated with close intermolecular contacts. All the intermolecular interactions reported earlier (C12-H12B…O2A, C15A-H15B…O3A, C43B-H43B…O1A for **4**; C23-H23A…O2 for **5**; short contacts F6A…O2, F6B…O2, F2A…O3, F2B…O3 for **6**), are visible in these plots.

3.4. DFT calculations

To better understand the molecular and electronic structure of the range of Re(I) complexes studied, a density functional theory (DFT) study was conducted. In this

study, the range of complexes **1**-**6**, as well as the comparative complexes *fac*-[$ReCO_3$(acac)(L)] (L = H_2O (**7**), PCy_3 (**8**)) were considered. The DFT optimized geometries of the complexes are shown in Figure 6. Generally, a good correlation between the theoretical and experimental geometries (SCXRD) is observed in bond distances and angles (Table 5). Furthermore, minimal variation in coordination and conformational isomers are notable, for example, different orientations of the cyclohexyl groups of the phosphine ligand. The formation of the meridional (*mer*) isomer over the facial (*fac*) isomer is generally not observed experimentally, as confirmed by DFT studies where an increase of 27-56 $kJ.mol^{-1}$ is observed for the less favourable *mer* isomer over the *fac* isomer in complexes **1**-**8**.

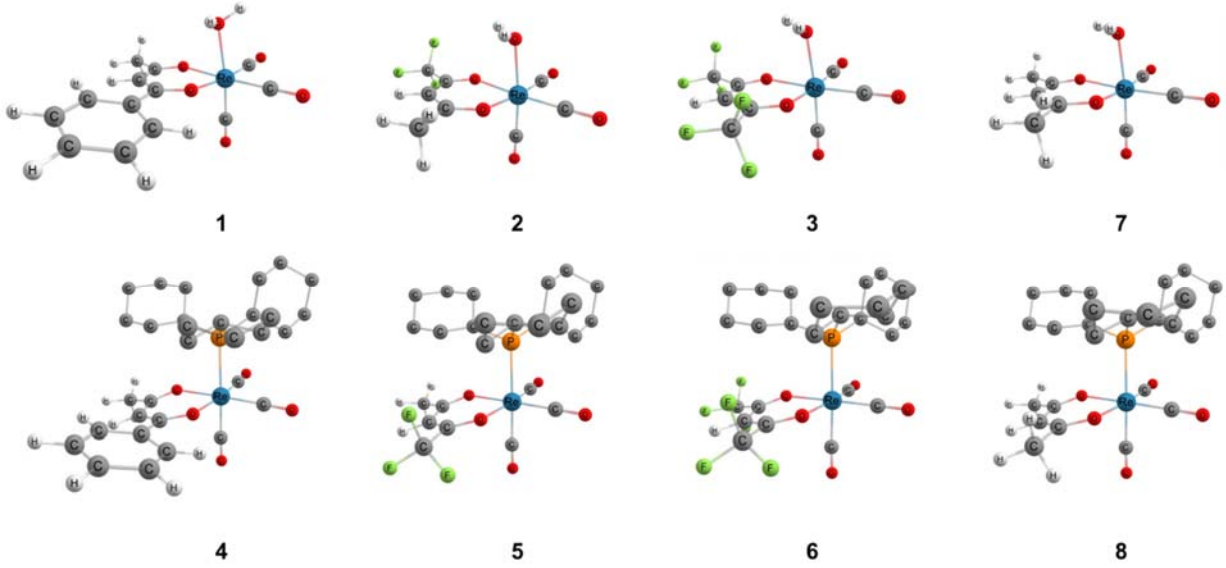

Figure 6: Optimized structures of complexes **1**-**8**. Colour code for atoms: Re (blue), P (orange), C (grey), O (red), F (green), H (white).

The theoretical and experimental Re-P and Re-O_{OO} bond distances compared well among complexes **1-8,** with the most significant deviation occurring for complex **4** (relative differences of 0.055 Å (Re-P) and 0.015 Å (average Re-O), with respect to molecule A of **4**), which supports the suitability of the theoretical model employed for analysis and comparison. Considering the optimised structures, a systematic elongation of the apical Re-C_{CO} bond length is seen as the electron-withdrawing nature of the β-diketonato ligands is increased (**8** ≈ **4** < **5** < **6**). In contrast, little change is observed in the average Re-C_{CO} bond length of the CO ligands *trans* to the oxygen donor atoms of the diketonato ligands as the ligands are varied. Omitting the outlier of

complex **8**, the reverse trend is the Re-P bond length increases as more electron-withdrawing β-diketonato ligands are employed: **4** > **5** > **6**. These observations correlate with the classical behaviour of π-acceptor ligands: donation of electron density from rhenium to the diketonato backbone as well as the apical carbonyl ligands results in the weakening/elongation of the Re-O and Re-C bonds, with a concomitant strengthening/shortening of the electron-donating ligands (PCy_3) bound to the Re centre. These effects are much less pronounced in the experimental structures. The bond angles of the various ligands to the metal centre compare relatively well with those obtained experimentally. However, it is seen that the optimised structures tend to conform closer to ideal octahedral (90°) geometries compared to those corresponding to the XRD structures, which is likely due to experimental factors including solvent and crystal packing effects.

Table 5: Structural comparison of complexes **1**-**8**.

Description		Complex[a]			
		4[b]	**5**	**6**	**8**
Bond distances (Å)	Re-C_{COap}[c]	1.955 (1.955)	1.948 (1.960)	1.956 (1.965)	1.937 (1.956)
	Re-C_{COeq}[c,d]	1.901 (1.917)	1.909 (1.915)	1.902 (1.915)	1.912 (1.917)
	Re-O_{OO}[d,e]	2.135 (2.149)	2.152 (2.167)	2.159 (2.172)	2.146 (2.158)
	Re-L[f]	2.515 (2.570)	2.532 (2.563)	2.517 (2.552)	2.545 (2.563)
Bond angles (°)	C_{COeq}-Re-C_{COap}[d]	88.82 (90.45)	88.43 (90.55)	88.47 (90.47)	87.75 (90.43)
	C_{COap}-Re-L	177.4 (178.3)	175.9 (178.5)	177.6 (178.6)	175.0 (178.5)
	O_{OO}-Re-L[d]	89.34 (89.68)	90.43 (90.52)	90.89 (90.69)	90.35 (90.07)
	O_{OO}-Re-C_{COeq}[d]	94.28 (92.34)	93.28 (92.47)	93.13 (92.70)	92.25 (92.25)
	O_{OO}-Re-C_{COap}[d]	90.19 (89.81)	90.41 (88.82)	89.56 (88.50)	92.20 (89.40)

[a] Experimental values (SCXRD), theoretical values (DFT) in parentheses. [b] Comparison with respect to molecule A of SCXRD structure of **4**. [c] CO ligands occupying the apical (ap) and equatorial (eq) positions with respect to the Re centre. [d] Average value reported. [e] OO = β-diketonato derivative ligand. [f] L = PCy_3 or H_2O ligand.

Comparison of the spectroscopic data (experimental and theoretical) was also included to evaluate further the effect of the β-diketonato ligands on specific measurables. The stretching frequencies of the carbonyl ligands (FT-IR

measurements) compare well with those calculated (unscaled values reported), especially for the more prominent frequencies (vco_{ap} > 2000 cm^{-1}). NMR spectroscopy was also considered: (i) ^{1}H NMR signals observed for the methine proton on the β-diketonato backbone of each of the complexes varied between δ_H 5.45 ppm (diketonato ligand bears electron-donating CH_3 groups, complex **8**) to δ_H 6.48 ppm (diketonato ligand bears electron-withdrawing CF_3 groups, complex **3**).

Table 6: Spectroscopic property comparison of complexes **1**-**8**.

Description		Complex[a]							
		1	**2**	**3**	**4**	**5**	**6**	**7**	**8**
FT-IR	v_{COap}[b]	2017 (2048)	2013 (2058)	2024 (2063)	2021 (2037)	2016 (2020)	2027 (2047)	2025 (2052)	2009 (2038)
	v_{COeq}[b]	1953 (1975)	1867 (1982)	1887 (1990)	1927 (1965)	1930 (1921)	1936 (1978)	1909 (1974)	1885 (1965)
	v_{COeq}	1904 (1959)	(1976)	(1984)	1909 (1943)	1892 (1899)	1904 (1955)	1884 (1969)	(1942)
^{1}H NMR	δ_H (OO)[c,d]	6.28 (6.60)	6.10 (6.39)	6.48 (6.53)	6.17 (6.49)	5.86 (5.91)	6.25 (6.54)	5.69 (5.90)	5.45 (5.71)
^{13}C NMR	δ_C (COeq)	190.3 (197.3)	198.7 (196.8)	196.5 (196.7)	191.4 (198.4)	206.5 (198.4)	(195.0)	190.22 (196.8)	197.7 (198.1)
	δ_C (COap)	197.7 (200.8)	199.1 (200.1)	210.3 (201.1)	181.7 (188.3)	191.9 (187.4)	174.1 (184.5)	199.0 (200.7)	189.4 (187.5)
	δ_C (COeq)	(196.9)	198.5 (196.7)	-	(197.4)	197.0 (197.6)	-	-	192.7 (197.3)
	δ_C (OO)[e]	96.7 (96.3)	98.9 (97.1)	94.2 (97.1)	99.0 (96.2)	98.5 (96.5)	92.1 (93.3)	103.5 (101.5)	102.5 (100.4)
^{31}P NMR	δ_C (PCy_3)	-	-	-	21.5 (19.3)	22.7 (20.6)	23.7 (21.5)	-	21.9 (20.7)

[a] Experimental values. Theoretical values (DFT, scaled) in parentheses. [b] CO ligands occupying the apical (ap) and equatorial (eq) positions with respect to the Re centre. [c] OO = β-diketonato derivative ligand. [d] Centre proton of RCOC*H*COR'. [e] Centre carbon of RCO*C*HCOR'.

The corresponding calculated values show a similar effect of the electron-withdrawing/donating character of the diketonato ligand where the same signals were calculated to be δ_H 5.71 ppm (complex **8**) and 6.53 ppm (complex **3**). (ii) The carbonyl carbon signals in the ^{13}C NMR spectra of **1**-**8** revealed downfield signals of δ_C 174.1-210.3 ppm for the various apical and equatorial carbonyl ligands. This correlated well with the calculated values of δ_C 187.4-201.1 ppm appearing in a narrower range. Closely related values for the methine carbon on the diketonato backbone were also observed, for example, comparing the experimental values δ_C 96.7 ppm (most upfield signal, complex **1**) and 103.5 ppm (most downfield signal, complex **7**) with the corresponding theoretical values of δ_C 96.3 ppm (complex **1**) and 101.5 ppm (complex **7**). (iii) Experimentally obtained ^{31}P NMR spectra of **4**-**6** and **8** compared relatively well

with those calculated and fell in the narrow ranges of 21.5-23.7 ppm (experimental) versus 19.3-21.5 (theoretical).

The thermodynamic stability and tendency for the complexes **4**-**6** and **8** to form *via* substitution of the corresponding aqua complexes (**1**-**3** and **7**) were also evaluated at the hand of comparison of the enthalpies of formation. This was calculated by considering the Gibbs free energy of each of the isolated complexes containing either an aqua (**1**-**3**, **7**) or a PCy_3 (**4**-**6**, **8**), followed by the summation of the individually calculated Gibbs free energies of the compounds as illustrated in the reaction of Figure 9. Following this method, it was observed that the systematic inclusion of more electron-withdrawing groups (CF_3) allowed for a stronger binding of the added PCy_3 ligand. Hence, more energy is released in the formation of the corresponding complexes. For complex **8** containing the most electron donating diketonato ligand in the range (acac), the most energy is required to substitute the aqua ligand (complex **7**) for a PCy_3 ligand (complex **8**).

Table 7: Thermodynamic properties of complexes **4**-**6**, and **8**.

Description	Complex			
	4	**5**	**6**	**8**
Gibbs free energy ($\times 10^6$ kJ.mol^{-1})	-5.26	-5.53	-6.32	-4.75
Formation enthalpy[a] (kJ.mol^{-1})	-474.18	-560.91	-802.70	-158.53

[a] Difference in the sum of the Gibbs free energy of the products and the sum of the Gibbs free energy of the reagents according to the reaction shown in Figure 9.

The rhenium atom as an electropositive atom is essentially charged (+1) and possesses a d^6 electron configuration (octahedral) with two available high-spin e_g orbitals, namely $d_{x^2-y^2}$ and d_{z^2}. The molecular orbital diagrams of representative complexes **3**, **6**-**8** are shown in Figure 7. Since the lowest energy state is a singlet state, each complex occupies three orbitals, containing an α and a β electron. The energy levels of interest (HOMO-5 to LUMO+5) of the phosphine complexes (**6**, **8**) are, in general, more compact as opposed to those of the aqua complexes (**3**, **7**). This is despite a slightly smaller energy gap ($E_{HOMO} - E_{LUMO}$) observed for **3** (3.45 eV) and **7** (4.12 eV), as opposed to the corresponding complexes **6** (3.47 eV) and **8** (4.20 eV). A smaller energy gap usually indicates enhanced reactivity or lowered stability.

Therefore, the stabilization of the rhenium centre by means of the electron donating PCy_3 as opposed to OH_2 is anticipated.

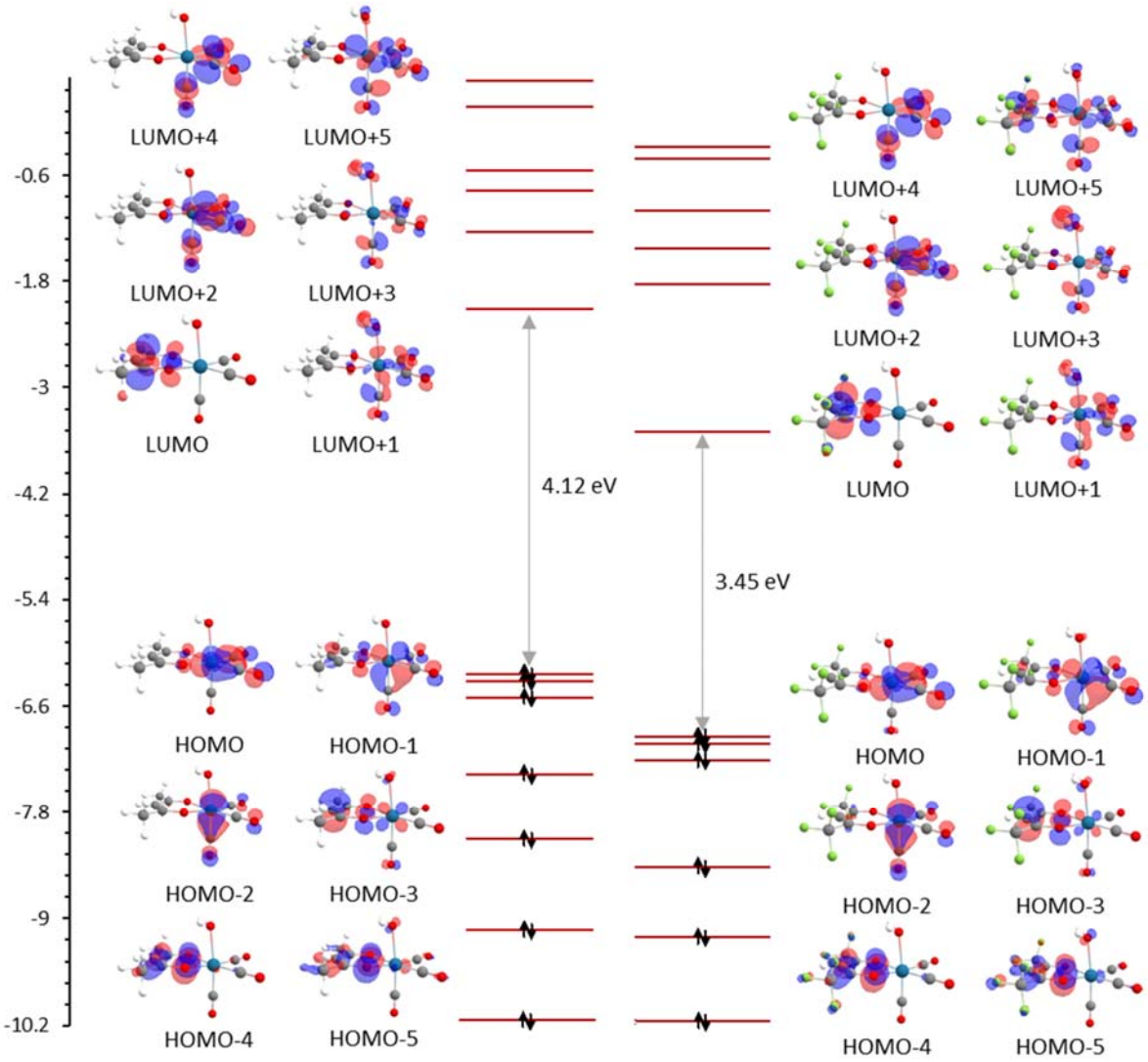

Figure 7: Molecular orbital diagram of the Re(I) aqua complexes **7** (left) and **3** (right). The %Re character is shown for selected orbitals, with the black arrows representing electrons in the filled orbitals. The HOMOs and LUMOs for each corresponding complex are also shown. Colour code for atoms: Re (blue), C (grey), O (red), F (green), H (white).

Substitution of the methyl groups on the acetylacetonato ligand for the electron-withdrawing CF_3 groups leads to an overall lowering in orbital energies (in particular the group of 8 orbitals of HOMO-3 up to LUMO+3), with a concomitant reduction in the associated energy gap (a decrease of 0.67 eV for **7** → **3**, and 0.73 eV for **8** → **6**). The reduction in energy gaps would, in turn, suggest a lowered reactivity of the fluoro-

containing diketonato Re(I) complexes where subsequent ligand substitution reactions are predicted to occur less readily.

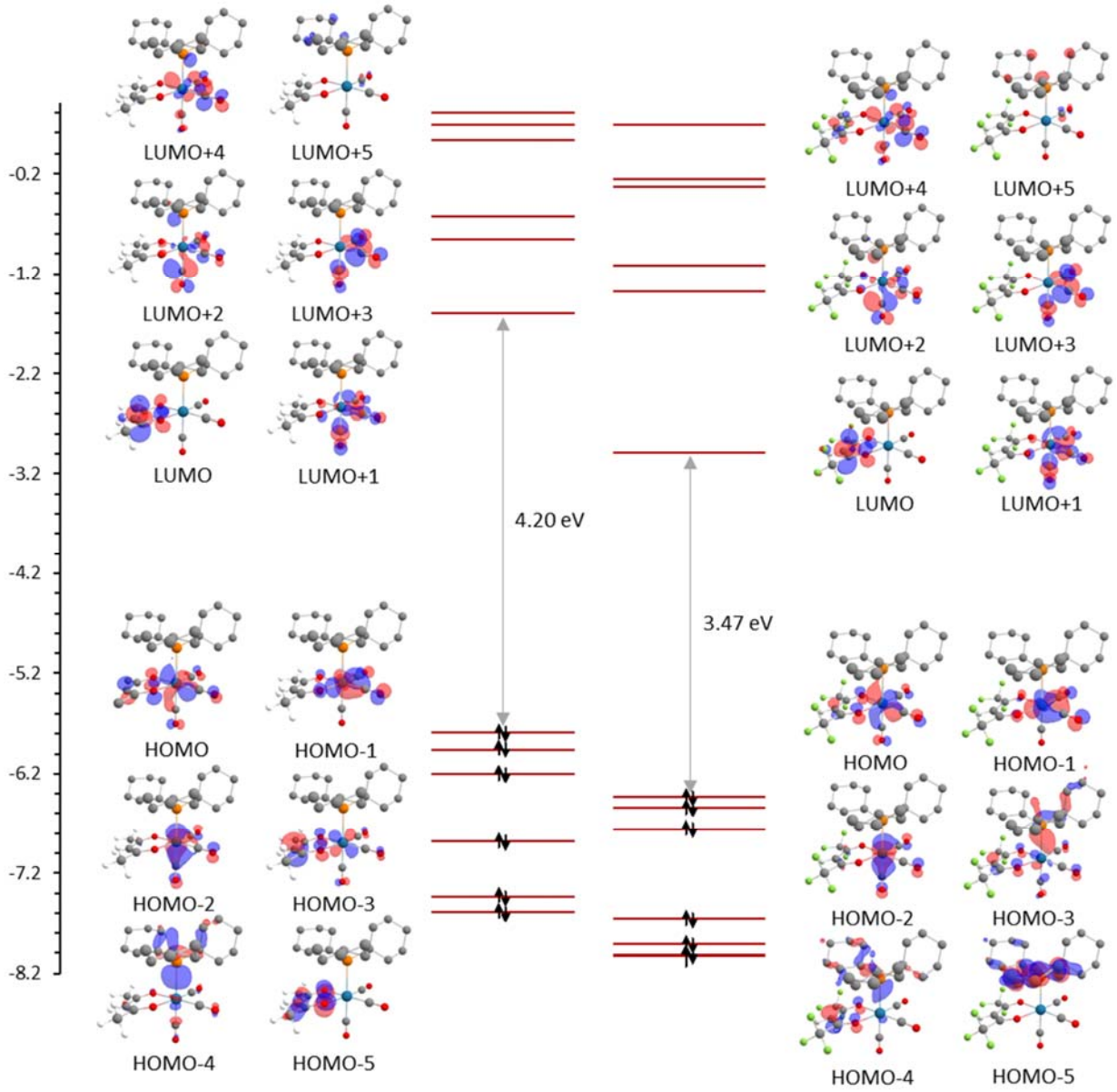

Figure 8: Molecular orbital diagram of the Re(I) phosphine complexes **8** (left) and **6** (right). The %Re character is shown for selected orbitals, with the black arrows representing electrons in the filled orbitals. The HOMOs and LUMOs for each corresponding complex are also shown. Colour code for atoms: Re (blue), P (orange), C (grey), O (red), F (green), H (white).

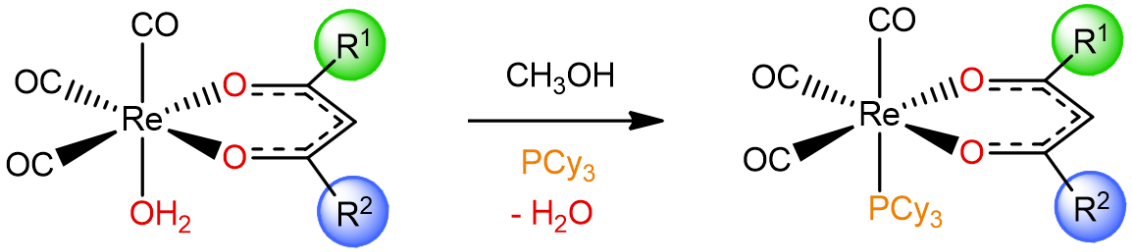

1	R^1 = Me; R^2 = Ph	**4**	R^1 = Me; R^2 = Ph
2	R^1 = Me; R^2 = CF_3	**5**	R^1 = Me; R^2 = CF_3
3	R^1 = CF_3; R^2 = CF_3	**6**	R^1 = CF_3; R^2 = CF_3
7	R^1 = Me; R^2 = Me	**8**	R^1 = Me; R^2 = Me

Figure 9: Synthesis of Re(I)-tricarbonyl complexes with coordinated monodentate tricyclohexylphosphine (**1**-**8**).

No other significant differences among the complexes are observed, apart from a minor difference in the ordering of the MOs of mainly Re-d, Re-π, and ligand-based character when comparing the aqua complexes (**3**, **7**) with the phosphine adduct complexes (**6**, **8**). Considering the complexes **3** and **6**-**8**: the top three occupied orbitals (HOMO, HOMO-1, HOMO-2) all have a large % Re character, whereas the three lowest-lying unoccupied orbitals (LUMO, LUMO+1, LUMO+2) have a markedly lower % Re character.

4. Conclusion

Three new crystal structures, **4**, **5,** and **6** were synthesised according to the '2+1' mixed ligand synthetic approach in high yield and purity. The use of this method display the ease of utilising this method as a preferred synthesis route. The synthesised complexes were characterised using spectroscopic methods IR, NMR, UV/Vis and SCXRD, confirming the molecular structures of the solid state complexes. The steric bulk of the axially coordinated PCy_3 ligand was calculated and expressed as the Tolman cone angle (θ) and computationally calculated Equivalence solid angle (θ°). In both methods a similar trend was displayed, which is that the steric bulk of the phosphine ligand on (**4**) is notably smaller than that coordinated on (**5**) and (**6**), indicating some steric interference from the phenyl ring on (**4**). The IR, SCXRD, DFT studies respectively revealed the electronic influence of the electronwithdrawing fluoro

atoms on the CO stretching frequency and elongated Re-O bond distances of (**6**). This comprehensive steric and electronic study adds to new knowledge regarding the correlations between computational and experimental investigations of Re(I) tricaronyl complexes with coordinated β-diketones.

ACKNOWLEDGMENTS

We would like to thank the National Research Foundation (Grant Nos. 129468 and 116246), Tshwane University of Technology, University of the Free State, South Africa, for financial support. Dr. Dumisani Kama and Christo van Staden are acknowledged for the data collection of the three crystal structures. Lesibana Jairus is acknowledged for the Equivalence angle calculations.

SUPPORTING INFORMATION

Supplementary crystallographic data: CSD 2126476, 2126478, and 2126477 contain the supplementary crystallographic data for **4**, **5**, and **6** and can be obtained free of charge from the Cambridge Crystallographic Data Centre via www.ccdc.cam.ac.uk/data_request/cif or by emailing data_request@ccdc.cam.ac.uk, or by contacting The Cambridge Crystallographic Data Centre, 12 Union Road, Cambridge CB2 1EZ, UK; fax: +44 1223 336033.

[1] H.C. Bertrand, S. Clède, R. Guillot, F. Lambert, C. Policar, Luminescence modulations of rhenium tricarbonyl complexes induced by structural variations, Inorg. Chem. 53(12) (2014) 6204–6223. https://doi.org/10.1021/ic5007007.

[2] C. Triantis, T. Tsotakos, C. Tsoukalas, M. Sagnou, C. Raptopoulou, A. Terzis, V. Psycharis, M. Pelecanou, I. Pirmettis, M. Papadopoulos, Synthesis and characterization of *fac*-[$M(CO)_3(P)(OO)$] and *cis-trans*-[$M(CO)_2(P)_2(OO)$] complexes (M = Re, ^{99m}Tc) with acetylacetone and curcumin as OO donor bidentate ligands, Inorg. Chem. 52(22) (2013) 12995–13003. https://doi.org/10.1021/ic401503b.

[3] J.R. Dilworth, S.J. Parrott, The biomedical chemistry of technetium and rhenium, Chem. Soc. Rev. 27 (1998) 43-55. https://doi.org/10.1039/A827043Z.

[4] S.S. Jurisson, J.D. Lydon, Potential technetium small molecule radiopharmaceuticals, Chem. Rev. 99(9) (1999) 2205-2218.

[5] K. Liepe, (188)Re-HEDP therapy in the therapy of painful bone metastases, World J. Nucl. Med. 17(3) (2018) 133-138.

[6] D.A. Kurtz, K.R. Brereton, K.P. Ruoff, H.M. Tang, G.A.N. Felton, A.J.M. Miller, J.L. Dempsey, Bathochromic shifts in rhenium carbonyl dyes induced through destabilization of occupied orbitals, Inorg. Chem. 57(9) (2018) 5389-5399. https://doi.org/10.1021/acs.inorgchem.8b00360.

[7] S.C. Marker, S.N. MacMillan, W.R. Zipfel, Z. Li, P.C. Ford, J.J. Wilson, Photoactivated in vitro anticancer activity of rhenium(I) tricarbonyl complexes, bearing water-soluble phosphines, Inorg. Chem, 57(3) (2018) 1311-1331. https://doi.org/10.1021/acs.inorgchem.7b02747.

[8] S. Sato, O. Ishitani, Photochemical reactions of *fac*-rhenium(I) tricarbonyl complexes and their application for synthesis, Coord. Chem. Rev. 282-283 (2015) 50-59.

[9] M. Wenzel, M.Patra, C.H.R. Senges, I. Ott, J.J. Stepanek, A. Pinto, P. Prochnow, C. Vuong, S. Langklotz, N. Metzler-Nolte, J.E. Bandow, Analysis of the mechanism of action of potent antibacterial hetero-tri-organometallic compounds: a structurally new class of antibiotics, ACS Chem. Biol. 8(7) (2013) 1442-1450. https://doi.org/10.1021/cb4000844.

[10] M. Patra, M. Wenzel, P. Prochnow, V. Pierroz, G. Gasser, J.E. Bandow, N. Metzler-Nolte, An organometallic structure-activity relationship study reveals the essential role of a $Re(CO)_3$ moiety in the activity against gram-positive pathogens including MRSA, Chem. Sci. 6 (2015) 214-224.

[11] D. Siegmund, N. Lorenz, Y. Gothe, C. Spies, B. Geissler, P. Prochnow, P. Nuernberger, J.E. Bandow, N. Metzler-Nolte, Benzannulated Re(I)–NHC complexes: synthesis, photophysical properties and antimicrobial activity, Dalton Trans. 46 (2017) 15269-15279.

[12] K. Schindler, F. Zobi, Photochemistry of rhenium(i) diimine tricarbonyl complexes in biological applications, Chimia 75 (2021) 837-844. doi:10.2533/chimia.2021.837.

[13] M.Sagnou, D. Benaki, C. Triantis, T. Tsotakos, V. Psycharis, C.P. Raptopoulou, I. Pirmettis, M. Papadopoulos, M. Pelecanou, Curcumin as the OO bidentate ligand in “2+1” complexes with the $[M(CO)_3]^+$ (M = Re, ^{99m}Tc) tricarbonyl core for radiodiagnostic applications, Inorg. Chem. 50 (2011) 1295-1303.

[14]A. Shegani, C. Triantis, B.A. Nock, T. Maina, C. Kiritsis, V. Psycharis, C. Raptopoulou, I. Pirmettis, F. Tisato, M.S. Papadopoulos, Rhenium(I) tricarbonyl complexes with (2-hydroxyphenyl) diphenylphosphine as PO bidentate ligand, Inorg. Chem. 6 (2017) 8175-8186.

[15] R. Alberto, R. Schibli, R. Waibel, U. Abram, A.P. Schubiger, Basic aqueous chemistry of $[M(OH_2)_3(CO)_3]^+$ (M=Re, Tc) directed towards radiopharmaceutical application, Coord. Chem. Rev. 190-192 (1999) 901-919.

[16] M. Riondato, D. Camporese, D. Martín, J. Suades, A. Alvarez-Larena, U. Mazzi, Synthesis and characterisation of $[Re(CO)_3(SS)(P)]$ complexes: a [2+1] concept for 99mTc- and 188Re-radiopharmaceutical applications, Eur. J. Inorg. Chem. 44 (2005) 4048-4055.

[17] S.C. Marker, S.N. MacMillan, W.R. Zipfel, Z. Li, P.C. Ford, J.J. Wilson, Photoactivated in vitro anticancer activity of rhenium (I) tricarbonyl complexes bearing water-soluble phosphines, Inorg. Chem. 57(3) (2018) 1311-1331.

[18] T.R. Hayes, B.B. Kasten, C.L. Barnes, P.D. Benny, Rhenium and technetium bi- and tricarbonyl complexes in a new strategy for biomolecule incorporation using click chemistry, Dalton Trans. 43 (2014) 6998-7001.

[19] P.D. Benny, G.A. Fugate, A.O. Barden, J.E. Morley, E. Silva-Lopez, B. Twamley, Metal-assisted in situ formation of a tridentate acetylacetone ligand for complexation of fac-$Re(CO)_3^+$ for radiopharmaceutical applications, Inorg. Chem. 47 (2008) 2240-2242.

[20] M. Schutte, G. Kemp, H.G. Visser, A. Roodt, Tuning the reactivity in classic low-spin d6 rhenium(I) tricarbonyl radiopharmaceutical synthon by selective bidentate ligand variation (L,L'-Bid; L,L' = N,N', N,O, and O,O' donor atom sets) in fac-$[Re(CO)_3(L,L'\text{-Bid})(MeOH)]^n$ complexes, Inorg. Chem. 50 (2011) 12486-12498.

[21] R. Alberto, R. Schibli, P.A. Schubiger, U. Abram, T.A. Kaden, Reactions with the technetium and rhenium carbonyl complexes $(NEt_4)_2[MX_3(CO)_3]$. Synthesis and structure of $[Tc(CN\text{-}But)_3(CO)_3](NO_3)$ and $(NEt_4)[Tc_2(\mu\text{-}SCH_2CH_2OH)_3(CO)_6]$, Polyhedron 15(7) (1996) 1079-1089.

[22] S.-P. Bruker, Version 7.12 (including XPREP). Bruker AXS Inc., Madison, Wisconsin, USA, 2004.

[23] A. Altomare, M.C. Burla, M. Camalli, G.L. Cascarano, C. Giacovazzo, A. Guagliardi, A.G.G. Moliterni, G. Polidori, R. Spagna, SIR97: A new tool for crystal structure determination and refinement, J. Appl. Cryst. 32(1) (1999) 115-119.

[24] L.J. Farrugia, WinGX suite for small-molecule single-crystal crystallography, J. Appl. Cryst. 32(4) (1999) 837-838.

[25] G. Sheldrick, Program for the refinement of crystal structures. Shelxl97, 1997.

[26] K. Brandenburg, M. Brendt, DIAMOND, Release 2.1 d. Crystal Impact GbR, Bonn, Germany, 2000.

[27] A.D. Becke, Becke's three parameter hybrid method using the LYP correlation functional, J. Chem. Phys. 98 (1993) 5648-5652.

[28] C.Y.W. Lee, R.G. Parr, Development of the Colle-Salvetti conelation energy formula into a functional of the electron density, Phys. Rev. B 37 (1988). 785-789.

[29] F. Neese, The ORCA program system. WIREs Comput Mol Sci. 2 (2012) 73-78.

[30] F. Weigend, R. Ahlrichs, Balanced basis sets of split valence, triple zeta valence and quadruple zeta valence quality for H to Rn: design and assessment of accuracy, Phys. Chem. Chem. Phys. 7 (2005) 3297-3305.

[31] K. Eichkorn, O. Treutler, H. Öhm, M. Häser, R. Ahlrichs, Auxiliary basis sets to approximate coulomb potentials, Chem. Phys. Lett. 240 (1995) 283-290.

[32] F. Neese, F. Wennmohs, A. Hansen, U. Becker, Efficient, approximate and parallel Hartree–Fock and hybrid DFT calculations. A 'chain-of-spheres' algorithm for the Hartree–Fock exchange, Chem. Phys. Lett. 356 (2009) 98-109.

[33] J.R. Cheeseman, G.W. Trucks, T.A. Keith, M.J. Frisch, A comparison of models for calculating nuclear magnetic resonance shielding tensors, J. Chem. Phys.104 (1996) 5497-5509.

[34] P.Gao, J. Zhang, H. Chen, A systematic benchmarking of ^{31}P and ^{19}F NMR chemical shift predictions using different DFT/GIAO methods and applying linear regression to improve the prediction accuracy, Int. J. Quant. Chem. 121 (2021) e26482.

[35] E. Benassi, Benchmarking of density functionals for a soft but accurate prediction and assignment of ^{1}H and ^{13}C NMR chemical shifts in organic and biological molecules, J. Comput. Chem. 38 (2017) 87-92.

[36] M.W. Lodewyk, M. R. Siebert, D.J. Tantillo, Computational prediction of ^{1}H and ^{13}C chemical shifts: a useful tool for natural product, mechanistic, and synthetic organic chemistry, Chem. Rev. 112 (2012) 1839-1862.

[37] G.A. Zhurko, ChemCraft, Version 1.8 (build 610), http://www.chemcraftprog.com
[38] A.-L. Manicum, O, Alexander, M. Schutte-Smith, H.G. Visser, Synthesis, characterization and substitution reactions of fac-[Re(O,O′-bid)(CO)3(P)] complexes, using the "2+ 1" mixed ligand model, J. Mol. Struct.1209 (2020) 127953.

[39] A.-L. Manicum, M. Schutte-Smith, G. Kemp, H.G. Visser, Illustration of the electronic influence of coordinated β-diketone type ligands: A kinetic and structural study, Polyhedron 85 (2015) 190-195.

[40] A.-L.E. Manicum, M. Schutte-Smith, H.G. Visser, The synthesis and structural comparison of fac-$[Re\ (CO)_3]^+$ containing complexes with altered β-diketone and phosphine ligands, Polyhedron 145 (2018) 80-87.

[41] M. Schutte, A. Roodt, H.G. Visser, Coordinated aqua vs methanol substitution kinetics in fac-Re(I) tricarbonyl tropolonato complexes, Inorg. Chem. 51(21) (2012) 11996-12006.

[42] A.-L.E. Manicum, M. Schutte-Smith, O. Alexander, L. Twigge, A. Roodt, H.G. Visser, First kinetic data of the CO substitution in fac-[Re (L, L′-Bid)(CO) 3 (X)] complexes (L, L′-Bid= acacetylacetonate or tropolonate) by tertiary phosphines PTA and PPh3: synthesis and crystal structures of water-soluble rhenium (I) tri-and dicarbonyl complexes with 1, 3, 5-triaza-7-phosphaadamantane (PTA), Inorg. Chem. Commun. 101 (2019) 93-98.

[43] C.A. Tolman, Steric effects of phosphorus ligands in organometallic chemistry and homogeneous catalysis, Chem. Rev. 77(3) (1977) 313-348.

[44] I.A. Guzei, M. Wendt, An improved method for the computation of ligand steric effects based on solid angles, Dalton Trans. 33 (2006) 3991-3999.

[45] V.L. Gantsho, M. Dotou, M. Jakubaszek, B. Goud, G. Gasser, H.G. Visser, M. Schutte-Smith, Synthesis, characterization, kinetic investigation and biological evaluation of Re(i) di- and tricarbonyl complexes with tertiary phosphine ligands, Dalton Trans. 49(1) (2020) 35-46.

[46] M. Schutte-Smith, A. Roodt, H.G. Visser, Ambient and high-pressure kinetic investigation of methanol substitution in fac-[Re(Trop)$(CO)_3$(MeOH)] by different monodentate nucleophiles, Dalton Trans. 48(27) (2019) 9984-9997.

[47] M. Schutte-Smith, S.C. Marker, J.J. Wilson, H.G. Visser, Aquation and anation kinetics of rhenium(I) dicarbonyl complexes: relation to cell toxicity and bioavailability, Inorg. Chem. 59(21) (2020) 15888-15897.

[48] P.R. Spackman, M.J. Turner, J.J. McKinnon, S.K. Wolff, D.J. Grimwood, D. Jayatilaka, M.A. Spackman, CrystalExplorer: a program for Hirshfeld surface analysis, visualization and quantitative analysis of molecular crystals, J. Appl. Crystallogr. 54(3) (2021) 1006-1011.

[49] M.A. Spackman, D. Jayatilaka, Hirshfeld surface analysis, CrystEngComm 11(1) (2009) 19-32.